

Dynamic covalent networks with tunable dynamicity by mixing acylsemicarbazides and thioacylsemicarbazides

Citation for published version (APA):

Sarkar, R., Majumdar, S., Kuil, S., Mallens, J., van der Tol, J. J. B., Sijbesma, R. P., Heuts, J. P. A., & Palmans, A. R. A. (2023). Dynamic covalent networks with tunable dynamicity by mixing acylsemicarbazides and thioacylsemicarbazides. *Journal of Polymer Science*, 61(13), 1335-1347. <https://doi.org/10.1002/pol.20230068>

DOI:

[10.1002/pol.20230068](https://doi.org/10.1002/pol.20230068)

Document status and date:

Published: 01/07/2023

Document Version:

Publisher's PDF, also known as Version of Record (includes final page, issue and volume numbers)

Please check the document version of this publication:

- A submitted manuscript is the version of the article upon submission and before peer-review. There can be important differences between the submitted version and the official published version of record. People interested in the research are advised to contact the author for the final version of the publication, or visit the DOI to the publisher's website.
- The final author version and the galley proof are versions of the publication after peer review.
- The final published version features the final layout of the paper including the volume, issue and page numbers.

[Link to publication](#)

General rights

Copyright and moral rights for the publications made accessible in the public portal are retained by the authors and/or other copyright owners and it is a condition of accessing publications that users recognise and abide by the legal requirements associated with these rights.

- Users may download and print one copy of any publication from the public portal for the purpose of private study or research.
- You may not further distribute the material or use it for any profit-making activity or commercial gain
- You may freely distribute the URL identifying the publication in the public portal.

If the publication is distributed under the terms of Article 25fa of the Dutch Copyright Act, indicated by the "Taverne" license above, please follow below link for the End User Agreement:

www.tue.nl/taverne

Take down policy





If you believe that this document breaches copyright please contact us at:

openaccess@tue.nl

providing details and we will investigate your claim.

RESEARCH ARTICLE

Dynamic covalent networks with tunable dynamicity by mixing acylsemicarbazides and thioacylsemicarbazides

Ramkrishna Sarkar^{1,2}  | Soumabrata Majumdar³ | Sierd Kuil¹ |
Jorg Mallens¹ | Joost J. B. van der Tol¹ | Rint P. Sijbesma³  |
Johan P. A. Heuts³  | Anja R. A. Palmans¹ 

¹Supramolecular Chemistry and Catalysis, Laboratory of Macromolecular and Organic Chemistry & Institute for Complex Molecular Systems, Eindhoven University of Technology, P.O. Box 513, Eindhoven, 5600 MB, The Netherlands

²Department of Chemistry, Indian Institute of Technology (IIT) Kanpur, Kanpur, 208016, India

³Supramolecular Polymer Chemistry, Laboratory of Macromolecular and Organic Chemistry & Institute for Complex Molecular Systems, Eindhoven University of Technology, P.O. Box 513, Eindhoven, 5600 MB, The Netherlands

Correspondence

Johan P.A. Heuts, Supramolecular Polymer Chemistry, Laboratory of Macromolecular and Organic Chemistry & Institute for Complex Molecular Systems, Eindhoven University of Technology, P.O. Box 513, Eindhoven 5600 MB, The Netherlands.
Email: j.p.a.heuts@tue.nl

Anja R. A. Palmans, Supramolecular Chemistry and Catalysis, Laboratory of Macromolecular and Organic Chemistry & Institute for Complex Molecular Systems, Eindhoven University of Technology, P.O. Box 513, Eindhoven 5600 MB, The Netherlands.
Email: a.palmans@tue.nl

Funding information

The Netherlands Organization for Scientific Research, Grant/Award Numbers: 731.016.202, 713.016.003

Abstract

Dynamic covalent networks (DCNs) use chemical bonds that break and reform at appropriate processing conditions to allow reconfiguration of the networks. Recently, the acylsemicarbazide (ASC) motif has been added to the repertoire of such dynamic covalent bonds, which is capable of hydrogen bonding as well as dynamic bond exchange. In this study, we show that its sulfur congener, thioacylsemicarbazide (TASC), also acts as a dynamic covalent bond, but exchanges at a slower rate than the ASC moiety. In addition, siloxane-based DCNs comprising either ASC or TASC motifs or a varying composition of both show tunable relaxation dynamics, which slow down with an increasing amount of TASC motifs. The reduction in stress relaxation goes hand in hand with a reduction of creep in the network and can be tuned by the ASC/TASC ratio. All networks are readily processed using compression molding and dissolve when treated with excess hydrazide in solution. The ability to control network properties and creep in dynamic covalent polymeric networks by small changes in the molecular structure of the dynamic bond allows a generalized synthetic approach while accommodating a wide temperature window for application.

KEYWORDS

acylsemicarbazide, dynamic covalent bond, dynamic covalent networks, hydrogen bonding, thioacylsemicarbazide

Ramkrishna Sarkar and Soumabrata Majumdar contributed equally to this study.

This is an open access article under the terms of the [Creative Commons Attribution](https://creativecommons.org/licenses/by/4.0/) License, which permits use, distribution and reproduction in any medium, provided the original work is properly cited.

© 2023 The Authors. *Journal of Polymer Science* published by Wiley Periodicals LLC.

1 | INTRODUCTION

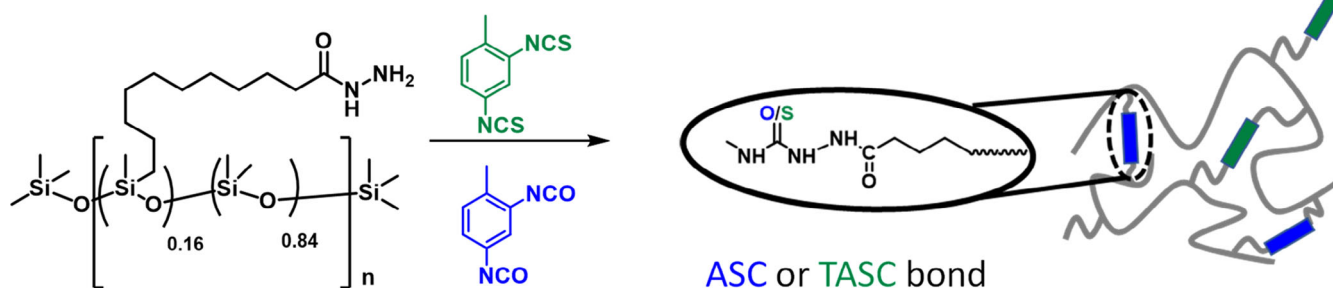
The search for materials that combine the excellent material properties of thermosets but are at the same time reconfigurable like thermoplastics has resulted in the development of dynamic covalent networks (DCNs).^{1–4} Herein, the chemical bonds holding the network together are no longer static and permanent, but dynamic, where they break and reform at appropriate processing conditions. The use of non-covalent bonds,^{5,6} dynamic covalent bonds,^{7–9} and combinations thereof^{10,11} has been explored in detail to achieve such dynamic properties. These investigations not only elucidated the different mechanisms by which bond exchange reactions can occur,¹² either associative or dissociative, but also highlighted the importance of the nature of the chemical bond,^{5,13} the network topology,^{14,15} and the time scales at which relaxation processes occur.^{1,3,16,17} Non-covalent bonds such as hydrogen bonds, for example, show fast relaxation processes at higher temperatures, whereas those of their dynamic covalent counterparts are much slower. As a result, the combination of the two has been receiving attention because of an enhancement of material properties which includes material strength and toughness, self-healing, and stimuli responsiveness.^{11,18–20}

In this respect, we were inspired by the acylsemicarbazide (ASC) bond (Scheme 1). ASCs are capable of multiple hydrogen bonding and, at the same time, show a tunable dynamic covalent bond character.²¹ Formed by the reaction of an isocyanate and a hydrazide, the ASC motif has slowly penetrated the world of polymeric materials over the last decade,^{21–25} with the first preparation of ASC-based polymers dating back to 1958.²⁶ Lehn and coworkers replaced traditionally used urethanes in linear polymer chains with ASCs and showed that the polymers formed films with elastic and self-healing properties.²⁴ Later, Palanisamy and coworkers used the ASC motif to create organogelators, which showed hydrogen-bonded networks in selected solvents.^{23,27} In 2020, Zuilhof, Xia,

and coworkers reported the use of ASCs in DCNs with impressive solid state material properties in combination with full recyclability and superb healing properties.²¹ In addition to forming dynamic hydrogen bonds, these ASC-based networks showed the ability to dynamically exchange covalent bonds.

A remaining challenge with the application of DCNs as a direct substitute for classical thermosets is material creep, which limits their applicability at higher temperatures. Several strategies can address creep, such as controlling the concentration of reactive groups,²⁸ utilizing dynamic chemistries with high activation energy,²⁹ introducing permanent crosslinks into the network,^{30,31} combining dynamic covalent bonds that show different relaxation times,^{32,33} or combining dynamic covalent chemistry with supramolecular interactions.¹⁰ Inspired by the work of Zuilhof and Xia, and motivated by the intriguing possibilities offered by changing “O” to its higher chalcogen “S”, we became interested in the thioacylsemicarbazide (TASC) motif. The TASC motif is expected to act as a dynamic covalent bond, similar to ASC. Currently, there are, to our knowledge, no data reported in the literature on hydrogen-bond formation, dynamic covalent bond exchange, and DCNs based on the TASC motif. Given the differences between C=O and C=S bonds,³⁴ and isocyanates being more reactive than isothiocyanates,^{35,36} we expected the chemical reactivity of the ASC and TASC motifs to be different, and thereby the kinetics of dynamic bond exchange reactions. In addition, to differences observed between ureas and thioureas,^{37,38} and amides and thioamides,^{39–42} we also expected the hydrogen bonding between ASC-ASC and TASC-TASC moieties to be different.

In this work, we combine two congenial chemistries with distinctly different exchange kinetics to address the problem of high temperature creep in DCNs while avoiding complicated procedures for material synthesis. We first report the dynamic bond exchange in small molecules bearing (T)ASC bonds and then apply the system in siloxane-based networks that comprise either ASC,



SCHEME 1 Synthesis scheme to siloxane-based networks comprising either ASC, TASC or both dynamic covalent bonds.

TASC, or a combination of the two as the dynamic covalent bond for network formation (Scheme 1). We identify how a small change in molecular structure affects bond exchange dynamics with concomitant changes in stress relaxation and creep; these processes correlate well with the amount of TASC bonds in the network and present a convenient handle to tune material properties.

2 | RESULTS AND DISCUSSION

2.1 | Bond exchange and hydrogen bonding in (T)ASC-based model compounds

We started our investigations by assessing the rate differences of bond exchange reactions in model compounds **1–4** comprising either ASC or TASC bonds (see Figure 1A for chemical structures). For this, the appropriate model compounds were mixed in DMSO-*d*₆ and the exchange between the (T)ASC bond with a hydrazide was followed with ¹H-NMR as a function of time. Since exploratory experiments showed that TASC compounds were exchanging slower, we selected 120 °C for ASC and the slightly higher temperature of 130 °C for TASC to have manageable time scales for the exchange reactions (Figures S1 and S2). It was previously reported that the exchange reaction for ASC proceeds via a dissociative mechanism, therefore the data were fit assuming first-order kinetics.²¹ The first-order rate coefficients *k*₁ of hydrazide-(T)ASC exchange are shown in Figure 1A. Even at 130 °C, the TASC reacts about 3 times more

slowly than the ASC with a hydrazide at 120 °C. Mixing ASC/ASC model compounds at 130 °C shows that exchange still occurs, but it takes longer to reach equilibrium (Figure S3). When mixing TASC/TASC, the reaction suffered from side reactions and overlapping NMR resonances (data not shown). We also mixed model ASC compound **1** with TASC **4** at 130 °C (Figure 1B). In this case, the rate of exchange was at the same time scale as for TASC with hydrazide, requiring 50 h to almost reach equilibrium (Figure S4). The latter result highlights that compounds comprising ASC and those with TASC can also exchange with each other.

The bulk IR spectra of aliphatic ASC and TASC model compounds **1** and **2** were measured to investigate the presence of hydrogen bonds in the solid state (Figure 1C). Whereas ASC **1** shows three defined NH stretch vibrations ($\nu(\text{NH})$) at 3325, 3200, and 3098 cm⁻¹, TASC **2** shows $\nu(\text{NH})$ at 3297 and 3198 cm⁻¹. The narrow and well resolved NH stretch vibrations are indicative of the presence of ordered hydrogen bonds, both for ASC and TASC model compounds.^{24,43} Interestingly, the NH stretch vibrations are blue-shifted for TASC **2** compared to the ASC **1**. This is in analogy to trithioamides and triamides, where the presence of “S” causes a blueshift in the NH stretch vibration.⁴¹ Likely, the more polarized C–S bond makes sulfur a better hydrogen-bond acceptor, and therefore, the formed hydrogen bonds are slightly stronger.^{41,44} In addition, the C=O stretch at 1660 cm⁻¹ for the ASC **1** red-shifts to 1686 cm⁻¹ for the TASC **2**. The additional peak at 1191 cm⁻¹ can likely be attributed to the C=S bond in **2**. The aromatic model compounds **3,4** show a more complex pattern of the NH stretch

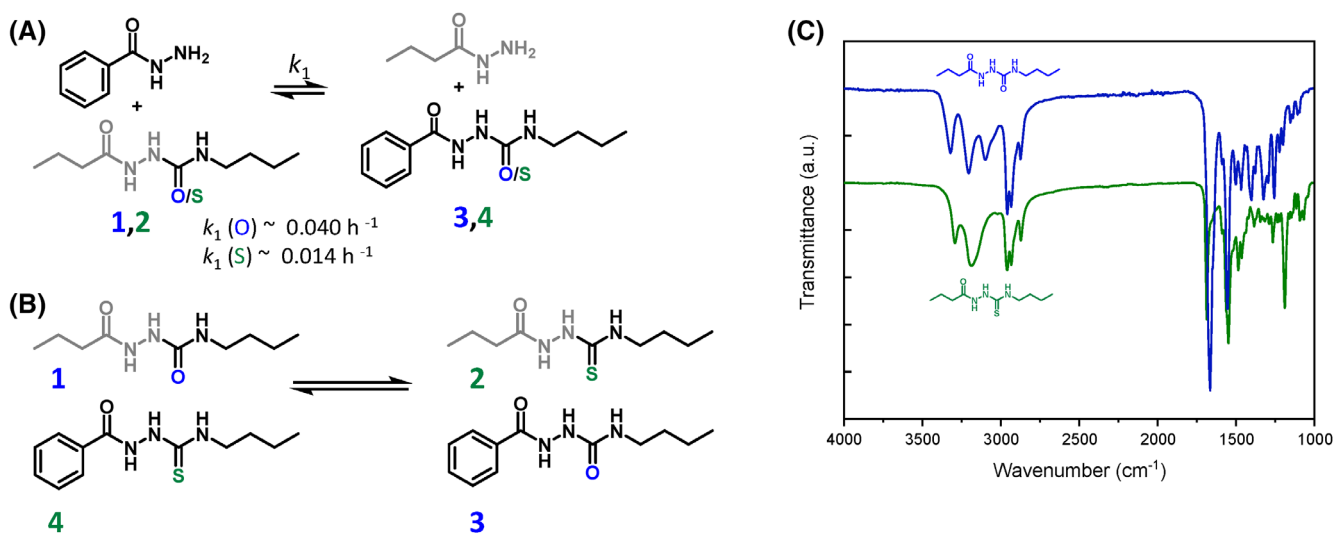


FIGURE 1 (A) Chemical structures of (T)ASC and hydrazide model compounds and *k*₁ of exchange reaction in DMSO at 120 or 130 °C for ASC and TASC, respectively; (B) TASC-ASC exchange at 130 °C of compounds **1,4** affording compounds **2,3**; (C) IR spectra of solid **1** (in blue) and **2** (in green) at room temperature.

vibrations, but a similar blue shift for the TASC 4 derivative compared to the ASC derivative 3 is observed (Figure S5).

2.2 | Synthesis and characterization of (T)ASC-based DCNs

Following the promising results for ASC and TASC bond exchange in the model compounds, we continued our investigations with the preparation of DCNs. Siloxane-based networks comprising ASC and/or TASC bonds (Figure 2A) were prepared starting from commercially available pHMS-co-pDMS ($M_n = 1.9\text{--}2\text{ kg mol}^{-1}$) comprising around 15–18 mol% Si–H (pHMS) units. The Si–H bonds are known to easily react with alkenes in a Karstedt's catalyst mediated hydrosilylation reaction.^{45,46} The prepolymer pHMS-co-pDMS was first reacted with

methyl 10-undecenoate, followed by the conversion of all pendant methyl ester groups to hydrazides by reacting with hydrazine. NMR and IR spectra showed that this reaction sequence readily affords the hydrazide pendant prepolymer in an overall 63% isolated yield in two steps (Figures S6 and S7). Subsequently, the hydrazide groups were reacted with either toluene-2,4-diisocyanate or toluene-2,4-diisothiocyanate using equimolar amounts of iso(thio)cyanate to hydrazide, to provide the crosslinked networks pDMS-100% ASC and pDMS-100% TASC (Figure 2A). Mixed networks were obtained by mixing the diisocyanate and diisothiocyanate in the desired molar ratio, with equimolar amounts of iso(thio)cyanate with respect to hydrazide, leading to networks pDMS-X% TASC. Here, X represents the molar percentage of TASC in the mixture; values of X were 12.5, 25, 50, and 75.

Since isothiocyanates react slower than isocyanates,^{35,36} the diisothiocyanate was added first and after a

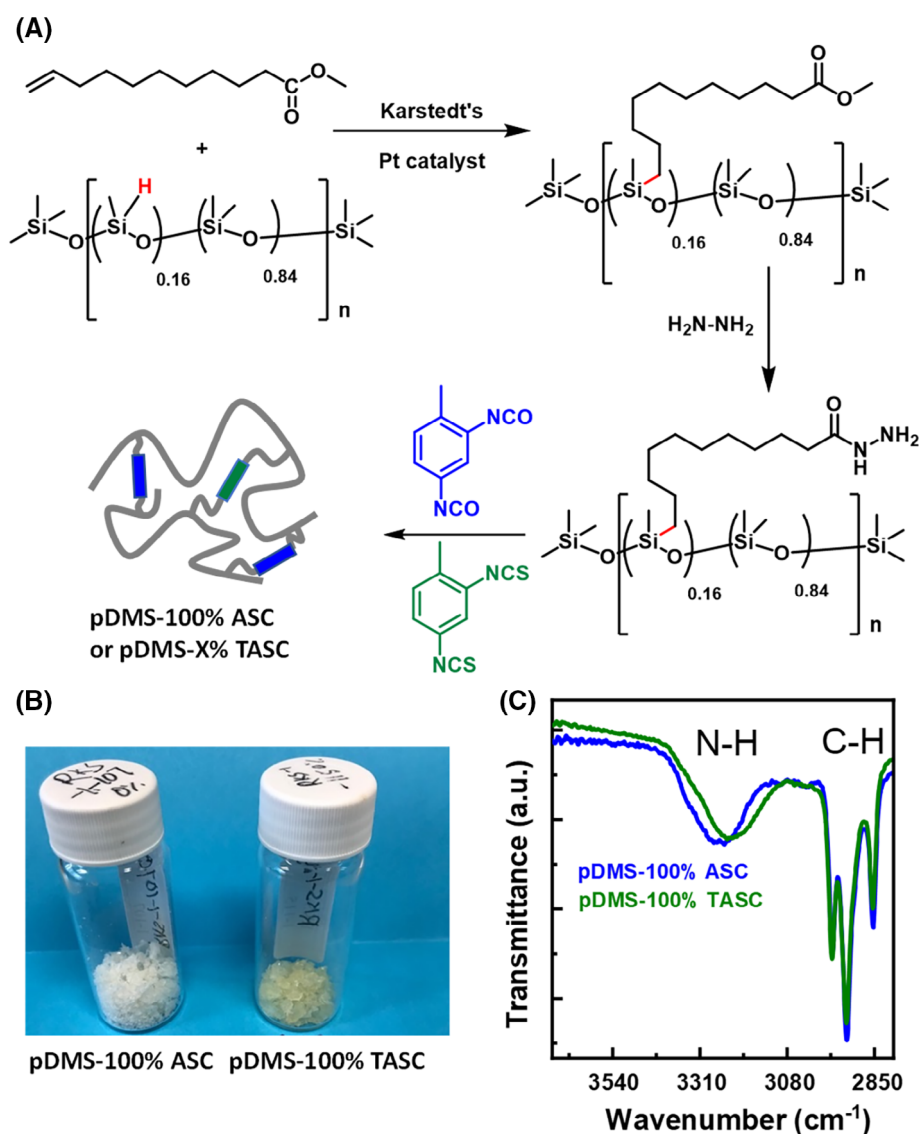


FIGURE 2 (A) Chemical structures of the starting siloxane polymer, intermediates, and final (T)ASC-based networks. (B) The appearance of pDMS-100% ASC and pDMS-100% TASC after isolation and drying; ASC networks are colorless whereas the TASC networks are yellowish to orange. (C) IR spectra of the NH stretch region of pDMS-100% ASC (in blue) and pDMS-100% TASC (in green) at room temperature.

homogeneous mixture was formed, the diisocyanate was quickly added. In contrast to the colorless ASC networks, the TASC networks were yellowish to orange (Figure 2B). All networks were insoluble in common organic solvents, with a gel fraction >0.94 when extracted with THF (Table S1). The as synthesized networks were characterized using thermogravimetric analysis (TGA), differential scanning calorimetry (DSC), and variable temperature FT-IR (VT-IR). TGA performed on pDMS-100% ASC and pDMS-100% TASC showed no noticeable weight loss up to 200 °C, revealing a good thermal stability (Figure S10). For the networks containing 75% and 100% TASC, DSC revealed a small exothermic peak around 0 °C, but no transitions were observed for the other networks, suggesting that these materials are fully amorphous at room temperature and higher (Figure S11).

The room temperature IR spectrum of pDMS-100% ASC shows one broad $\nu(\text{NH})$ at 3257 cm^{-1} and $\nu(\text{CO})$ at 1658 cm^{-1} (Figure 2C, full spectra in Figure S12), which is consistent with the presence of hydrogen bonds. A previous report on ASC-based networks with PPO as the soft block showed $\nu(\text{NH}) = 3325\text{ cm}^{-1}$ and $\nu(\text{CO})$ at 1640 cm^{-1} at room temperature.²¹ Based on the position of the NH stretch vibration, the hydrogen bonds in the siloxane-based system seem to be stronger as they appear at lower wavenumbers. The values in pDMS-100% TASC are blue shifted for $\nu(\text{NH}) = 3227\text{ cm}^{-1}$ and red-shifted for the $\nu(\text{CO}) = 1673\text{ cm}^{-1}$ (Figure 2C, full spectra in Figure S12). Also for the networks, the presence of “S” causes a blue-shift for $\nu(\text{NH})$ (around 30 cm^{-1}) and a redshift for $\nu(\text{CO})$. The broadness of the NH peak in the networks when compared to those of the model compounds 1–4 (Figure S13) suggests that the hydrogen bonds are more disordered, which is in line with the amorphous character of the networks. With increasing temperature, VT-IR showed a slight broadening of the NH stretch and a shift to higher wavenumbers, indicating the weakening of the hydrogen bonds for both networks (Figures S14 and S15).⁴⁷ Plotting the peak maximum of the NH stretch as a function of temperature for pDMS-100% ASC and pDMS-100% TASC shows that the temperature dependencies of both networks are the same as indicated by the similar slopes (Figure S16).⁴⁸ This suggests that the sensitivity of the hydrogen bonds to temperature is similar for both networks.

2.3 | Dynamic nature of the (T)ASC-based DCNs

To assess if ASC and TASC bonds were still capable of undergoing exchange reactions when embedded in the pDMS-based networks, we first conducted a dissolution experiment (Figure 3A,B). Upon treatment with excess

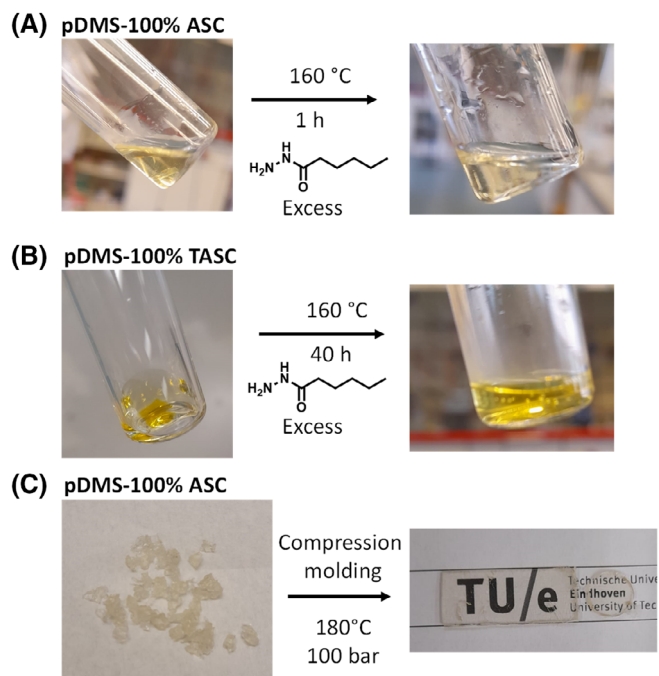


FIGURE 3 Images illustrating the complete dissolution of pDMS-100% ASC after 1 h (A) and pDMS-100% TASC after 40 h (B) when heated at 160 °C in pure hexanohydrazide. (C) Before (left) and after (right) compression molding of pDMS-100% ASC.

hexanohydrazide (nearly 20-fold excess with respect to the functional group) at 160 °C, pDMS-100% ASC and pDMS-100% TASC completely dissolved in 1 and 40 h, respectively. The dissolution of the pDMS networks in excess hydrazide highlights the presence of reactive and dynamic groups in the network that undergo exchange reactions wherein the dissolution time correlates with their exchange rates observed in small molecular (T)ASC model systems.

In addition, we evaluated if the synthesized networks can be processed into desired shapes using compression molding, which is a qualitative indication of dynamic rearrangements of the bonds within the material. At temperatures above 140 °C and at 100 bar, compression molding was indeed feasible for all obtained networks, including pDMS-100% TASC (Figures 3C and S9). The networks with >75% TASC bonds required a longer compression molding time (2–2.5 h) compared to those with 50% or less TASC bonds (1–1.5 h), which is in line with the slower exchange dynamics of the TASC bonds.

2.4 | DMTA analysis of (T)ASC-based DCNs

The thermo-mechanical properties of the networks were next studied by dynamic mechanical thermal analysis (DMTA), using compression molded rectangular

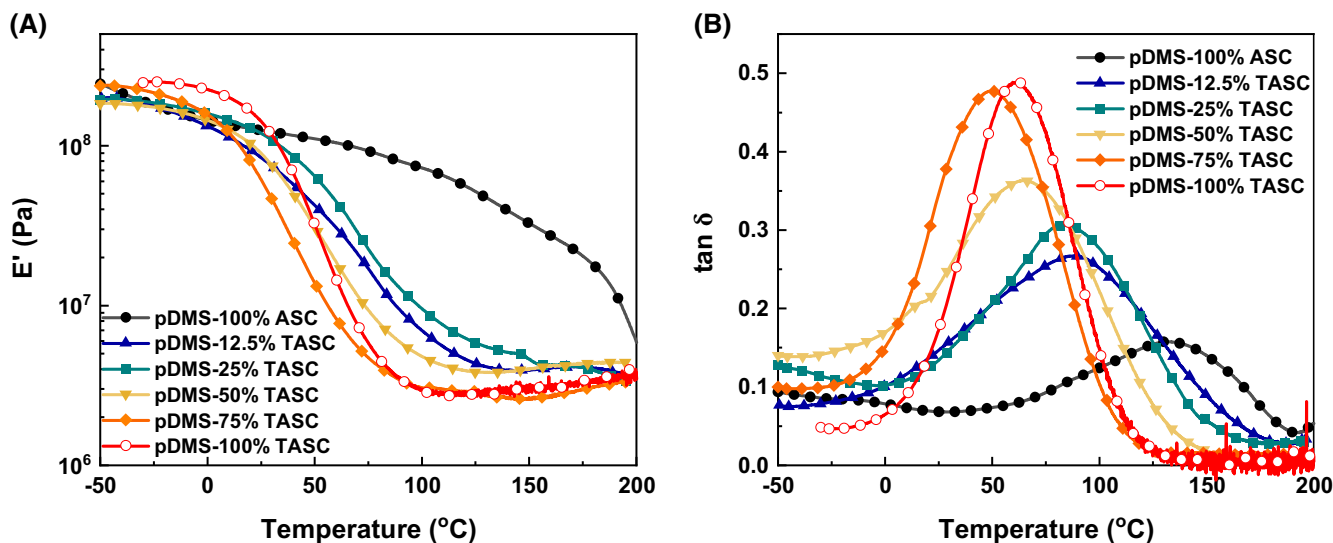


FIGURE 4 Dynamic mechanical thermal analysis under extension on the pDMS networks obtained after compression molding with variation in TASC content representing (A) the storage modulus (E') and (B) $\tan \delta$ as a function of temperature.

bar-shaped samples (Figure 4). Figure 4A shows the storage modulus E' as a function of temperature for the different networks. The DMTA curve of the ASC network shows a rather different behavior compared to the TASC comprising networks. The exact origin of this is currently unclear but we believe it is caused by network inhomogeneities. This could be a result of fast network formation with the isocyanates giving rise to a more heterogeneous network, which affords domains with different crosslink densities. The slower bond formation with isothiocyanates, may afford a more homogeneous network compared to the ASC network. In addition, $\tan \delta$, indicative for the glass transition temperature (T_g), was plotted as a function of temperature. Rather broad peaks are observed in Figure 4B, especially for networks comprising a high amount of ASC bonds. The ASC-based network shows a T_g of around 130 °C and the TASC-based network of around 60 °C. The T_g decreases with increasing amounts of TASC bonds in the networks to around 50 °C for pDMS-75% TASC (Table S2). The decrease in T_g could be due to a different packing of the hydrogen bonds in networks that comprise both TASC and ASC bonds, which may affect the mobility of the networks. The T_g 's of these siloxane-based networks are high compared to other systems based on pDMS,^{49,50} likely a result of the high crosslink density in these networks.⁵⁰

2.5 | Rheological characterization of (T)ASC-based DCNs

To get insights in the dynamic bond exchange in the networks, we performed rheology experiments. Step

transient rheology experiments were done on compression molded samples under shear at temperatures between 140 and 200 °C (Figure 5). Samples from pDMS-100% ASC showed almost complete relaxation of imposed stress at 200 °C within 300 s indicating the fast network rearrangement through bond exchange reactions at this temperature (Figure 5A). A small residual stress (R) of 5% was observed, the origin of which is currently unclear. The stress relaxation plots were fit with a stretched exponential function (Equation 1) to obtain the characteristic relaxation times (τ) (Table 1).^{7,51}

$$\frac{G(t)}{G(1s)} = \frac{R + e^{-(t/\tau)^\beta}}{R + e^{-(1/\tau)^\beta}} \quad (1)$$

The material showed faster relaxation rates at higher temperatures because of faster bond exchange kinetics. The stretch factor, β , which is often considered as an indication of the dispersity of a particular relaxation mode,^{52,53} was 0.4–0.5 suggesting a relatively broad distribution and thus a possibility of multiple relaxation modes in the material. Furthermore, the exchange within the hydrogen-bonded domains probably adds more relaxation modes. The characteristic relaxation times, obtained from the fit, were represented in an Arrhenius plot (Supporting Information, Equation S2) and the flow activation energy was determined to be 146 kJ/mol (Figure 5B). This value is significantly higher than the one of 100 kJ/mol reported previously for an ASC-based network based on PPO.²¹ Compared to other dynamic systems, this activation

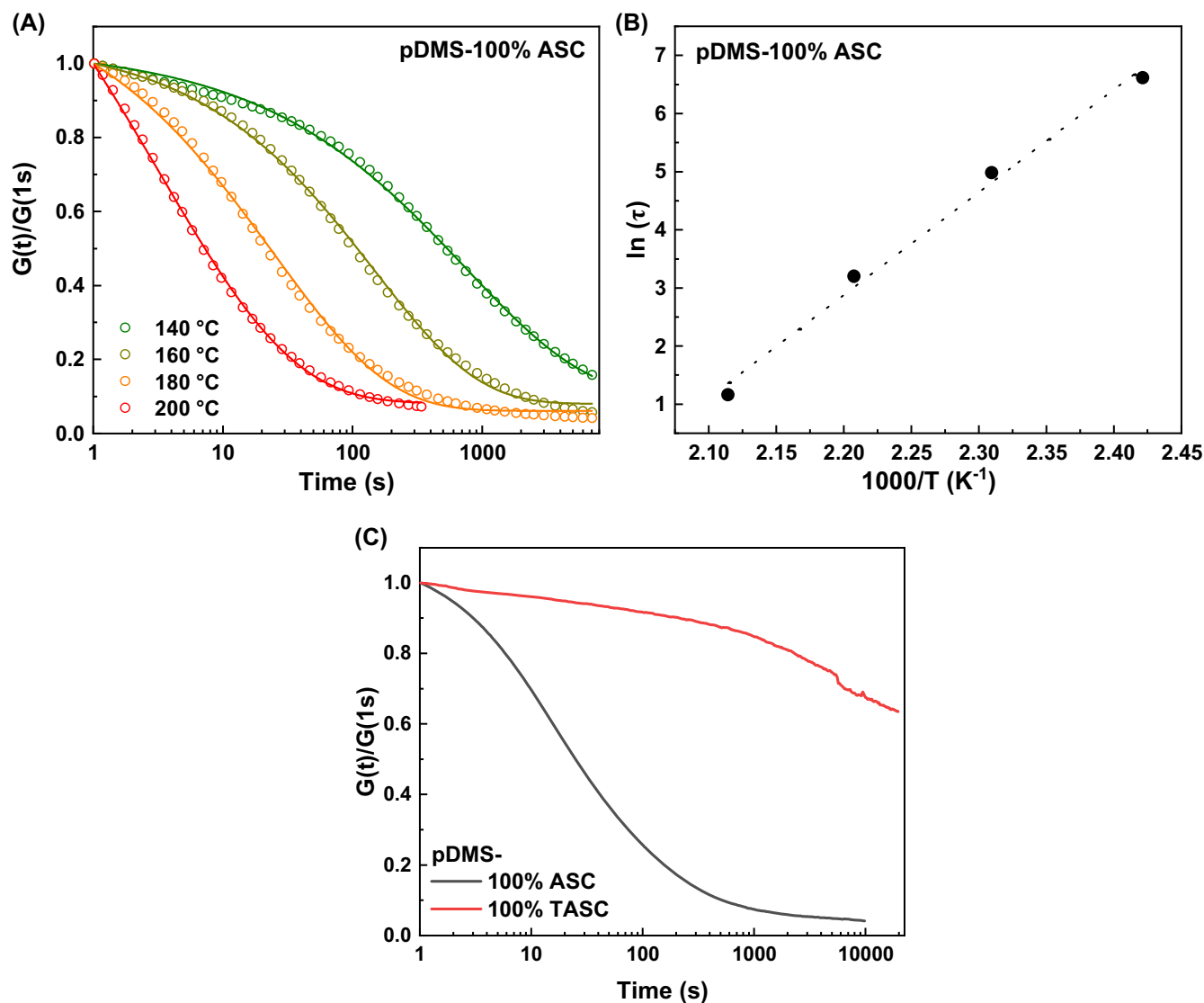


FIGURE 5 (A) Stress relaxation under shear with temperature variation on pDMS-100%ASC; under 5% strain. The solid lines represent the fitting using Equation 1; (B) Arrhenius plot for pDMS-100% ASC using the characteristic relaxation times derived from the stress relaxation experiment. The activation energy determined from the Arrhenius plot was 146 kJ/mol; (C) Comparison of stress relaxation rate between pDMS-100% ASC and pDMS-100% TASC networks at 180 °C (applied strain 5%).

TABLE 1 Fit parameters for the relaxation time (τ), stretch factor (β), and residual stress (R) derived from stress relaxation plots of pDMS-100%ASC.

Temperature [°C]	τ [s]	β [-]	R [%]
200	3	0.4	5
180	29	0.5	5
160	146	0.5	8
140	748	0.4	10

energy is higher than for some internally catalyzed transesterifications,^{54–56} vinylogous urethanes⁵⁷ and dioxoboranes,⁵⁸ similar to some metal-catalyzed transesterifications^{59–61} and triazolium systems,^{62,63}

but lower than systems based on transalkylation using 1,4-diazabicyclo[2.2.2]octane.⁶⁴

Figure 5C shows the comparison of stress relaxation rates between pDMS-100% ASC and pDMS-100% TASC at 180 °C. The stress relaxation rates for pDMS-100% TASC were significantly slower than for pDMS-100% ASC, and a characteristic relaxation time of about $253 \cdot 10^3$ s was estimated. The very slow stress relaxation of pDMS-100% TASC, which is consistent with the lower exchange rates in the model systems of the previous section, precludes an exact determination of its flow activation energy, but it is estimated to be well above 300 kJ/mol (see Supporting Information, Figures S17 and S18 for more details).

2.6 | Stress relaxation in mixed networks

Next, stress relaxation experiments were conducted on the mixed networks, pDMS-12.5%TASC to pDMS-75% TASC at 180 °C, and the results of these experiments are shown in Figure 6A. The data clearly show that an increase in TASC content results in a slower relaxation of the stresses, and that different relaxation times are present in the mixed networks. The observed increase in stress in the stress relaxation profile of pDMS-75% TASC is rather unexpected. Whereas this upturn was not caused by an experimental error as it was reproducible

for different samples of the same network, we have no explanation for it other than that some side reactions may be taking place.

Similar to what was done by Du Prez and coworkers,³³ we evaluated if the stress relaxation in the TASC containing networks (we excluded pDMS-75% TASC here because of the upturn) can be described by assuming a linear combination of the contributions of the fast mode (ASC bonds, $\tau = 29$ s at 180 °C) and the slow mode (TASC bonds, $\tau = 253 \cdot 10^3$ s at 180 °C), with contributions close to their respective mole fractions. We used Equation 2 to first “predict” the stress

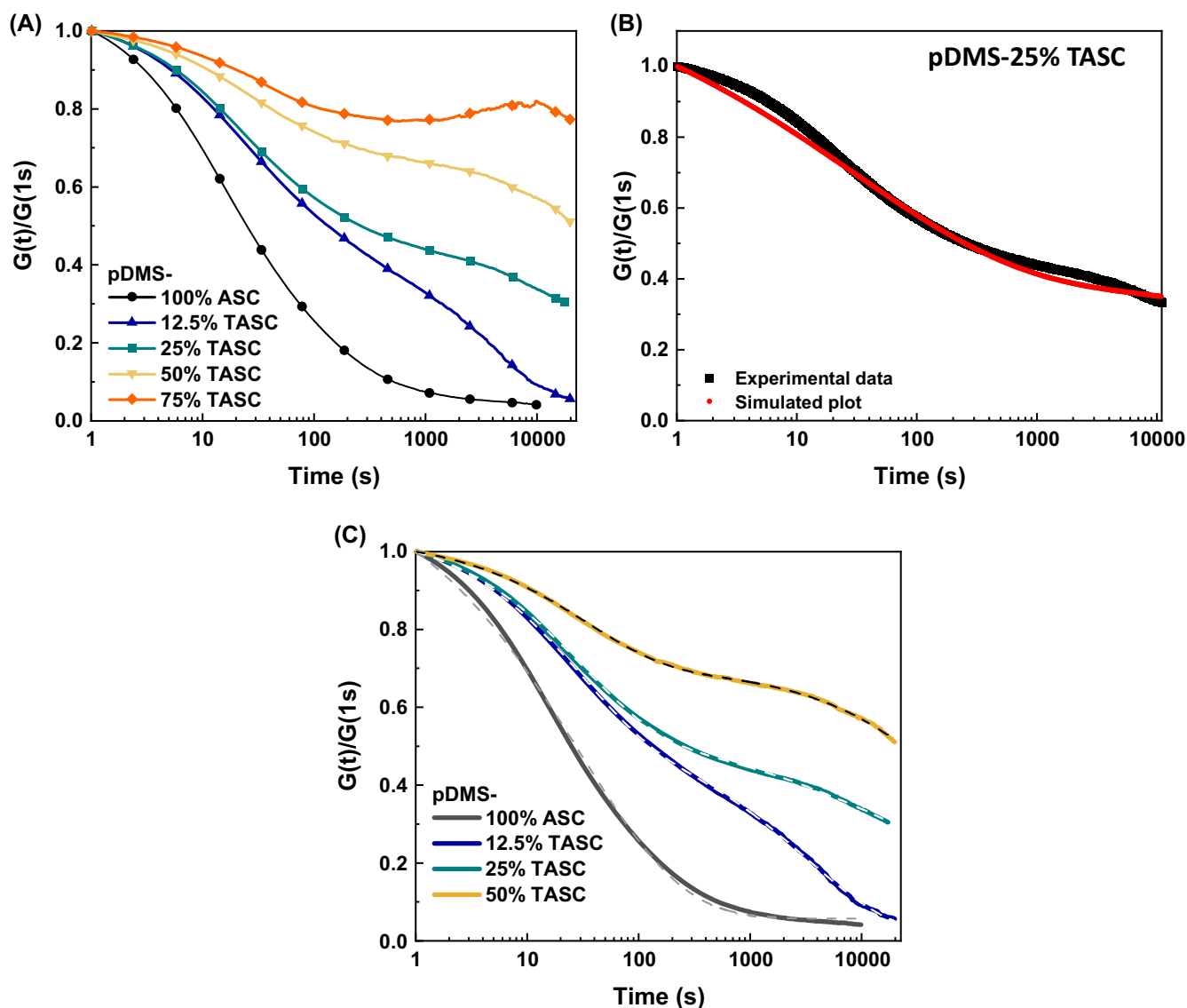


FIGURE 6 (A) Stress relaxation profile of the pDMS mixed networks recorded at 180 °C (with 5% strain) normalized at $t = 1$ s; (B) Overlay of predicted (red symbols, using Equation 2) and measured (black squares) stress relaxation profile of pDMS-25% TASC. The predicted stress relaxation profile is based on a linear combination of two relaxation mechanisms arising from ASC exchange and TASC exchange with contributions based on the molar ratio between ASC and TASC groups; (C) Stress relaxation profile of the pDMS-based mixed networks at 180 °C with fits using Equation 2.

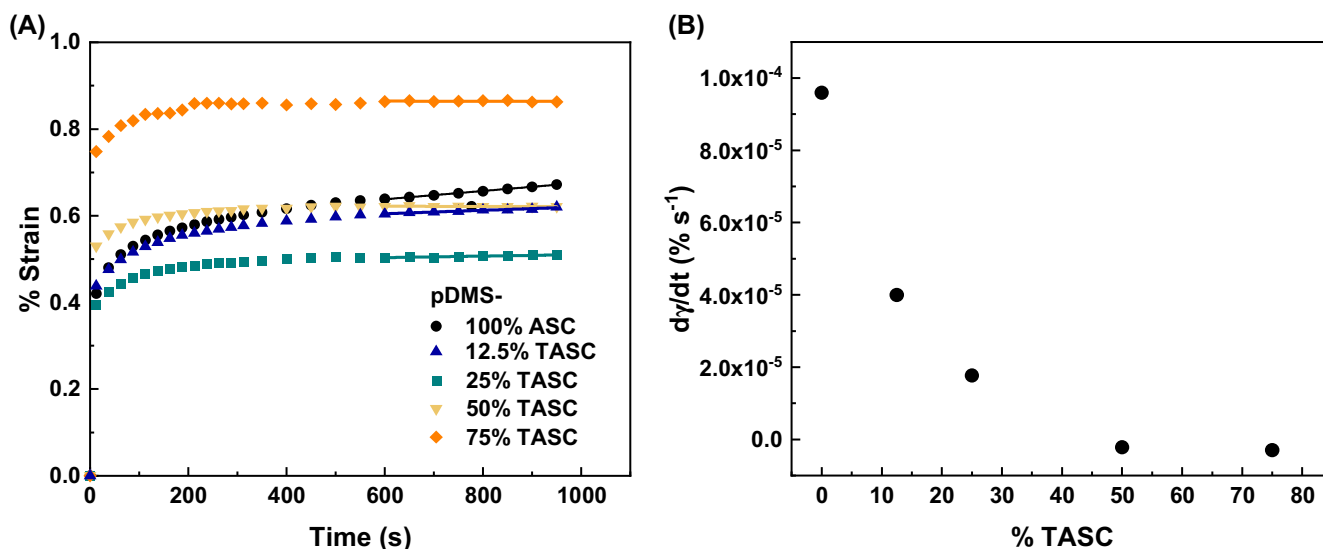


FIGURE 7 (A) Creep under shear at 180 °C (applied stress 5000 Pa) of pDMS networks with varying content of TASC linker. (B) Creep rates at 180 °C as obtained from the secondary phase in (A).

relaxations of the mixed networks. As an example, the result for pDMS-25% TASC is shown in Figure 6B (others are found in Figure S18, with a summary of all the used parameters in Table S3). Although there is no perfect overlap, these a priori predictions come close to the experimental curves, with the exception of the 12.5% TASC system, displaying more deviations (Figure S18). This suggests that the stress relaxation is mainly governed by these largely independent, separate modes.

$$\frac{G(t)}{G(1s)} = \frac{R + A1 \cdot e^{-(t/\tau_1)\beta_1} + (1 - A1) \cdot e^{-(t/\tau_2)\beta_2}}{R + A1 \cdot e^{-(1/\tau_1)\beta_1} + (1 - A1) \cdot e^{-(1/\tau_2)\beta_2}} \quad (2)$$

As shown in Figure 6C, the stress relaxation data for all networks except pDMS-75% TASC were subsequently fit using Equation 2, and the obtained fit parameters are summarized in Table S4. The fast relaxation time is found between 27 to 32 s for all networks, and is attributed to ASC exchange reactions. These similar values for all networks indicate that the fast relaxation is fairly independent of the amount of TASC bonds present in the network. The contribution of the fast mode goes down with increasing TASC content, but not proportionally (Table S4). The slow mode varies between $\sim 3 \times 10^3$ s and $\sim 159 \times 10^3$ s and is ascribed to TASC exchange. This value increases a factor of 50 with increasing amounts of TASC bonds from 12.5% to 50%, approaching the relaxation time of 253×10^3 s for the pure TASC network. These results suggest potential interactions between the two main modes of relaxation.

2.7 | Controlling creep in dynamic covalent networks

The slow exchange of TASC links in the network was then utilized to study the possibilities of controlling the creep resistance of the materials with (T)ASC bonds. Therefore, the networks were studied with an isothermal creep experiment at 180 °C (Figure 7A). The strain rate in the secondary creep phase, which is ascribed to the viscous flow of the material, was derived and is shown in Figure 7B. The strain rate decreases significantly with increasing TASC content in the network. The slightly negative values for the strain rates in the samples containing 50% and 75% TASC samples may be caused by possible side reactions, causing additional crosslinks and a small contraction against the applied stress. Overall, these results corroborate that a simple chemical modification allows to easily tune bond exchange dynamics, and hereby creep.

3 | CONCLUSIONS

In conclusion, model compounds comprising ASC or TASC bonds show pronounced differences in bond exchange kinetics, with TASC bonds exchanging at a slower rate than ASC bonds. In addition, an ASC comprising model compound exchanges with a TASC compound, which indicates that the difference in bond exchange dynamics does not hamper cross exchange. Our observations from model compound studies translate satisfactorily to the relaxation properties of the polymeric networks with ASC (pDMS-100% ASC) and TASC (pDMS-100% TASC) crosslinks, with

faster relaxation rates for the former. The pDMS-100% ASC network shows an activation energy of the flow of 146 kJ/mol, which is within the range of reported activation energies for other DCNs, whereas that of the pDMS-100% TASC shows a significantly higher activation energy, which we estimate to be around 300 kJ/mol. Stress relaxation in networks with increasing amounts of TASC bonds depended on the amount of TASC bonds. Although several types of bond relaxation processes are likely operative in the mixed networks, more TASC bonds in the networks result in slower relaxation dynamics. This reduction in stress relaxation is accompanied by a reduction in creep. The ability to control network properties and creep in DCNs by small changes in the molecular structure of the dynamic bond opens up novel opportunities for network design. This concept can be applied to many of the existing dynamic covalent links and can provide a general tool to tune network properties without much alteration of existing synthetic strategies.

4 | EXPERIMENTAL SECTION

4.1 | Materials and methods

Siloxane PDMS-*co*-PHMS (1.9–2 kDa with 15–18 mol% hydride) was purchased from Gelest, product code HMS-151. All solvents were purchased from Biosolve and were dried, where necessary, using an MBraun solvent (drying) purification system (MB SPS-800). Deuterated compounds were obtained from Cambridge Isotopes Laboratories. All the starting materials which include (thio)isocyanates, esters, hydrazine, benzohydrazide, and other reagents were purchased either from Sigma Aldrich or TCI. These were used as received. Karstedt's catalyst (in xylene, Pt ~2%) was purchased from Sigma Aldrich.

400 MHz Bruker Avance III spectrometer was utilized to record NMR spectra. The compounds (10–20 mg) were taken into a suitable deuterated solvent. Proton and carbon chemical shifts are reported in ppm (δ) downfield from tetramethylsilane (TMS) using the deuterated solvent resonance frequency as an internal standard. Peak multiplicities are abbreviated as s: singlet; d: doublet; t: triplet; q: quartet; p: pentet; m: multiplet; dd: double doublet; dt: double triplet and dq: double quartet. Differential scanning calorimetry (DSC) studies were carried out using a Q2000 DSC (TA instruments), calibrated with an indium standard. Typically, 4–6 mg compound was directly weighted into aluminum pans and hermetically sealed. Subsequently, the samples were heated above the melting point for the removal of the thermal history, followed by two heating and cooling cycles at a rate of 10 K min⁻¹ for the verification of the reproducibility. Unless otherwise

mentioned, all DSC curves represent the second heating/cooling cycle. TGA was performed in a Discovery TGA 550 (TA instruments) from 100 to 600 °C at a temperature ramp of 10 K min⁻¹. Perkin Elmer FT-IR Spectrum Two apparatus was used to record all room temperature IR. The variable temperature FT-IR studies were carried out utilizing the JASCO Tensor 27 with Pike ATR temperature unit. The solid samples were heated/cooled at a rate of 10 K min⁻¹. Materials were compression molded at 180 °C at 100 bar. Samples for the 100%, 87.5%, 75%, and 50% ASC-crosslinked materials were compression molded for 1–1.5 h and the 100% and 75% TASC crosslinked materials for 2.5 and 2 h, respectively. DMTA studies were performed under uniaxial oscillatory deformation using a DMA Q850 (TA instruments) on compression molded rectangular bars. Stress relaxation and creep were performed under shear on circular disks shaped compression molded samples using plate-plate geometry in a Discovery HR 20 (TA instruments).

4.2 | Synthesis of (T)ASC model compounds and networks

4.2.1 | General procedure for (thio)aclysemicarbazide synthesis

The desired hydrazide (4.4 mmol) was dissolved in a two-necked round bottom flask containing dry DCM (15 mL) and purged with argon for 10 min. Due to the solubility issues of the few hydrazides, a small amount of dry THF was added for its solubilization. The equimolar amount of (thio)isocyanate (4.4 mmol) was dissolved in dry DCM (3 mL) and added dropwise to the solution under vigorous stirring. The mixture was stirred overnight at room temperature. A white crystalline solid precipitation of the product formed immediately (within 5 min) for ASC compounds, whereas for TASC compounds, the precipitation of the product formed upon stirring the reaction overnight. Removal of the solvent under reduced pressure and drying of the residue under a high vacuum yielded the final product in near-quantitative yield. Unless specific reaction conditions and workup procedures are mentioned, the aforementioned procedures were followed.

4.2.2 | N-butyl-2-butyrylhydrazine-1-carboxamide (**1**)

The product was obtained as a white solid.

¹H NMR (δ , 400 MHz, DMSO-*d*₆): 9.36 (*d*, 1H, CH₂–CO–NH–NH–CO–NH), 7.57 (*d*, 1H, CH₂–CO–NH–NH–CO), 6.21 (*t*, 1H, CO–NH–CH₂),

2.99 (qua, 2H, CO—NH—CH₂—CH₂), 2.05 (*t*, 2H, CH₂—CH₂—CO), 1.51 (*m*, 2H, CH₃—CH₂—CH₂—CO), 1.35 (*qui*, 2H, NH—CH₂—CH₂—CH₂—CH₃), 1.25 (*m*, 2H, NH—CH₂—CH₂—CH₂—CH₃), 0.86 (*dt*, 6H, NH—CH₂—CH₂—CH₂—CH₃). ¹³C NMR (100 MHz, DMSO-*d*₆) δ 172.42, 158.65, 39.26, 35.55, 32.41, 20.03, 19.08, 14.09, 13.94.

4.2.3 | N-butyl-2-butyrylhydrazine-1-carbothioamide (2)

The product was obtained as a white solid.

¹H NMR (δ , 400 MHz, DMSO-*d*₆): 9.55 (*s*, 1H, NH), 9.02 (*s*, 1H, NH), 7.77 (*t*, 1H, CH₂—NH), 3.42 (*qua*, 2H, CH₂—NH), 2.09 (*t*, 2H, CH₂—CO), 1.49 (*m*, 4H, CH₂), 1.26 (*sex*, 2H, CH₂), 0.87 (*dt*, 6H, CH₃). ¹³C NMR (100 MHz, DMSO-*d*₆) δ (ppm): 182.02, 172.31, 43.74, 35.66, 31.36, 19.88, 18.50, 14.22, 14.09.

4.2.4 | 2-benzoyl-N-butylhydrazine-1-carboxamide (3)

The reaction was performed in THF. The product was obtained as a white solid.

¹H NMR (δ , 400 MHz, DMSO-*d*₆): 10.09 (*s*, 1H, NH), 7.88 (*d*, 2H, Ar—H), 7.78 (*s*, 1H, NH), 7.56 (*t*, 1H, Ar—H), 7.48 (*t*, 2H, Ar—H), 6.47 (*t*, 1H, NH—CH₂), 3.03 (*t*, 2H, 2H, NH—CH₂), 1.39 (*qui*, 2H, NH—CH₂CH₂), 1.29 (*sex*, 2H, NH—CH₂—CH₃), 0.87 (*t*, 3H, CH₃). ¹³C NMR (100 MHz, DMSO-*d*₆) δ 166.28, 158.32, 132.76, 131.59, 128.27, 127.53, 39.34, 32.00, 19.43, 13.73.

4.2.5 | 2-benzoyl-N-butylhydrazine-1-carbothioamide (4)

The product was obtained as a white solid.

¹H NMR (δ , 400 MHz, DMSO-*d*₆): 10.29 (*s*, 1H, NH), 9.22 (*s*, 1H, NH), 8.06 (*t*, 1H, NH—CH₂), 7.91 (*d*, 2H, Ar—H), 7.57 (*t*, 1H, Ar—H), 7.49 (*t*, 2H, Ar—H), 3.42 (*t*, 2H, NH—CH₂), 1.50 (*qui*, 2H, CH₂), 1.29 (*sex*, 2H, CH₂), 0.87 (*t*, 3H, CH₃). ¹³C NMR (100 MHz, DMSO-*d*₆) δ 182.00, 166.39, 133.00, 132.27, 128.77, 128.30, 43.88, 31.39, 19.93, 14.29.

4.2.6 | Synthesis of pDMA-100% ASC and pDMS-X% TASC

(A) PDMS-*co*-PHMS [16–18 mol% PHMS, M.W = 2 kDa] (20.0 g) and methyl 10-undecenoate (3 equivalents

compared to Si—H in the polymer) were taken in a 100 mL two neck round bottom flask containing 20 mL THF and the mixture were purged with argon for 30 min. The reaction mixture was placed in a preheated oil bath at 60 °C. Then, 500 μ L Karstedt's catalyst was added to it dropwise using a syringe and the mixture was left to stir overnight at 60 °C under argon. The progress of the reaction was monitored by ¹H NMR, which revealed the disappearance of the Si—H signal after the overnight reaction, revealing the completion of the reaction. The reaction mixture was allowed to cool at room temperature and washed with 150 mL (3 \times 50 mL) methanol for the removal of excess methyl undecanoate. The product, the siloxane polymer, which was in the sediment, was isolated by decantation. The polymer was dried under a high vacuum (\sim 1 mbar) to obtain a viscous liquid product with a nearly 76% yield.

(B) Then, 10 g of the parent PDMS-*co*-PHMS polymer grafted with methyl undecanoate was dissolved in a 30 mL THF/MeOH (ratio = 2:1 v:v) mixture. To the mixture, an excess hydrazine monohydrate (10 g) was added and the mixture was left to stir at room temperature under argon for 2 h, then the mixture was heated to 50 °C and was left to stir overnight. The progress of the reaction was monitored by ¹H NMR spectroscopy until the reaction was complete. The reaction mixture was decanted and the hydrazide functionalized siloxane polymer which was in the sediment part was dried under a high vacuum (<1 mbar) at 70 °C with 83% yield.

(C) A typical procedure proceeds as follows: the siloxane polymer with hydrazide pendants (3 g, 4.74 mmol hydrazides) was dissolved in dry THF (15 mL) and the solution was purged with argon under vigorous stirring for 30 min. Depending on the desired composition of the network, toluene-2,4-diisocyanate and/or toluene-2,4-diisothiocyanate (2.37 mmol in total) were dissolved in 2 mL dry THF separately. Under an argon atmosphere and vigorous stirring, the toluene-2,4-diisothiocyanate (TDIT) was added via a syringe. Once homogeneously mixed, it was followed by the quick addition of the toluene-2,4-diisocyanate (TDI). The gel formation occurred within 2–10 min at room temperature, depending upon the fraction TDIT; a higher amount of TDIT leads to a longer gelation time due to its slow reaction kinetics. The mixture was left to react at room temperature for 1 h after which it was heated to 50 °C and left overnight with argon flow. Finally, the vacuum drying of the network at 80 °C results in further curing and drying.

ACKNOWLEDGMENTS

This work was financially supported by The Netherlands Organization for Scientific Research (ECHO Grant 713.016.003, TA Grant 731.016.202).

ORCID

Ramkrishna Sarkar  <https://orcid.org/0000-0002-2887-2666>

Rint P. Sijbesma  <https://orcid.org/0000-0002-8975-636X>

Johan P. A. Heuts  <https://orcid.org/0000-0002-9505-8242>

Anja R. A. Palmans  <https://orcid.org/0000-0002-7201-1548>

REFERENCES

- [1] C. J. Kloxin, C. N. Bowman, *Chem. Soc. Rev.* **2013**, *42*, 7161.
- [2] P. R. Christensen, A. M. Scheuermann, K. E. Loeffler, B. A. Helms, *Nat. Chem.* **2019**, *11*, 442.
- [3] N. Zheng, Y. Xu, Q. Zhao, T. Xie, *Chem. Rev.* **2021**, *121*, 1716.
- [4] N. J. van Zee, R. Nicolaÿ, *Prog. Polym. Sci.* **2020**, *104*, 101233.
- [5] I. Sacligil, C. W. Barney, A. J. Crosby, G. N. Tew, *Soft Matter* **2022**, *18*, 4937.
- [6] C. Li, C. Wang, C. Keplinger, J.-L. Zuo, L. Jin, Y. Sun, P. Zheng, Y. Cao, F. Lissel, C. Linder, X.-Z. You, Z. Bao, *Nat. Chem.* **2016**, *8*, 618.
- [7] G. M. Scheutz, J. J. Lessard, M. B. Sims, B. S. Sumerlin, *J. Am. Chem. Soc.* **2019**, *141*, 16181.
- [8] P. Chakma, D. Konkolewicz, *Angew. Chem. Int. Ed.* **2019**, *58*, 9682.
- [9] S. Huang, X. Kong, Y. Xiong, X. Zhang, H. Chen, W. Jiang, Y. Niu, W. Xu, C. Ren, *Eur. Polym. J.* **2020**, *141*, 110094.
- [10] B. Zhang, Z. A. Digby, J. A. Flum, E. M. Foster, J. L. Sparks, D. Konkolewicz, *Polym. Chem.* **2015**, *6*, 7368.
- [11] Z. Wang, S. Gangarapu, J. Escorihuela, G. Fei, H. Zuilhof, H. Xia, *J. Mater. Chem. A* **2019**, *7*, 15933.
- [12] J. M. Winne, L. Leibler, F. E. Du Prez, *Polym. Chem.* **2019**, *10*, 6091.
- [13] A. Perego, F. Khabaz, *J. Polym. Sci.* **2021**, *59*, 2590.
- [14] Y. Gu, J. Zhao, J. A. Johnson, *Trends Chem.* **2019**, *1*, 318.
- [15] B. Soman, C. M. Evans, *Soft Matter* **2021**, *17*, 3569.
- [16] W. Denissen, J. M. Winne, F. E. Du Prez, *Chem. Sci.* **2016**, *7*, 30.
- [17] M. K. McBride, B. T. Worrell, T. Brown, L. M. Cox, N. Sowan, C. Wang, M. Podgorski, A. M. Martinez, C. N. Bowman, *Annu. Rev. Chem. Biomol. Eng.* **2019**, *10*, 175.
- [18] S. Yu, R. Zhang, Q. Wu, T. Chen, P. Sun, *Adv. Mater.* **2013**, *25*, 4912.
- [19] J. A. Neal, D. Mozhdghi, Z. Guan, *J. Am. Chem. Soc.* **2015**, *137*, 4846.
- [20] C. Zhang, Z. Yang, N. T. Duong, X. Li, Y. Nishiyama, Q. Wu, R. Zhang, P. Sun, *Macromolecules* **2019**, *52*, 5014.
- [21] D. Fu, W. Pu, J. Escorihuela, X. Wang, Z. Wang, S. Chen, S. Sun, S. Wang, H. Zuilhof, H. Xia, *Macromolecules* **2020**, *53*, 7914.
- [22] M. I. Shtil'man, O. Y. Fedotova, H. S. Kolesnikov, *Polym. Sci. U.S.S.R.* **1968**, *10*, 330.
- [23] S. Baddi, A. Palanisamy, *Eur. Polym. J.* **2018**, *99*, 90.
- [24] N. Roy, Ž. Tomović, E. Buhler, J.-M. Lehn, *Chem. Eur. J.* **2016**, *22*, 13513.
- [25] C. Fan, B. Liu, Z. Xu, C. Cui, T. Wu, Y. Yang, D. Zhang, M. Xiao, Z. Zhang, W. Liu, *Mater. Horiz.* **2020**, *7*, 1160.
- [26] T. W. Campbell, V. S. Foldi, J. Farago, *J. Appl. Polym. Sci.* **1958**, *II*, 155.
- [27] S. Baddi, S. S. Madugula, D. S. Sarma, Y. Soujanya, A. Palanisamy, *Langmuir* **2016**, *32*, 889.
- [28] F. Van Lijsebetten, K. De Bruycker, Y. Spiesschaert, J. M. Winne, F. E. Du Prez, *Angew. Chem. Int. Ed.* **2022**, *61*, e202113872.
- [29] L. Li, X. Chen, K. Jin, M. Bin Rusayyis, J. M. Torkelson, *Macromolecules* **2021**, *54*, 1452.
- [30] J. J. Cash, T. Kubo, D. J. Dobbins, B. S. Sumerlin, *Polym. Chem.* **2018**, *9*, 2011.
- [31] L. Li, X. Chen, K. Jin, J. M. Torkelson, *Macromolecules* **2018**, *51*, 5537.
- [32] L. Porath, J. Huang, N. Ramlawi, M. Derkaloustian, R. H. Ewoldt, C. M. Evans, *Macromolecules* **2022**, *55*, 4450.
- [33] F. Van Lijsebetten, K. De Bruycker, E. Van Ruymbeke, J. M. Winne, F. E. Du Prez, *Chem. Sci.* **2022**, *13*, 12865.
- [34] K. B. Wiberg, Y. Wang, *Arkivoc* **2011**, *2011*, 45.
- [35] K. B. Wiberg, Y. G. Wang, S. J. Miller, A. L. A. Puchlopek, W. F. Bailey, J. D. Fair, *J. Org. Chem.* **2009**, *74*, 3659.
- [36] L.-T. T. Nguyen, M. T. Gokmen, F. E. Du Prez, *Polym. Chem.* **2013**, *4*, 5527.
- [37] Y. Yanagisawa, Y. Nan, K. Okuro, T. Aida, *Science* **2018**, *359*, 72.
- [38] J. Xu, P. Chen, J. Wu, P. Hu, Y. Fu, W. Jiang, J. Fu, *Chem. Mater.* **2019**, *31*, 7951.
- [39] Y. Nakano, T. Hirose, P. J. M. Stals, E. W. Meijer, A. R. A. Palmans, *Chem. Sci.* **2012**, *3*, 148.
- [40] P. J. M. Stals, M. M. J. Smulders, R. Martín-Rapún, A. R. A. Palmans, E. W. Meijer, *Chem. Eur. J.* **2009**, *15*, 2071.
- [41] T. Mes, S. Cantekin, D. W. R. Balkenende, M. M. M. Frissen, M. A. J. Gillissen, B. F. M. de Waal, I. K. Voets, E. W. Meijer, A. R. A. Palmans, *Chem. Eur. J.* **2013**, *19*, 8642.
- [42] C. Nieuwland, C. Fonseca Guerra, *Chem. Eur. J.* **2022**, *28*, e202200755.
- [43] N. Roy, E. Buhler, J.-M. Lehn, *Chem. Eur. J.* **2013**, *19*, 8814.
- [44] M. J. Janssen, J. Sandström, *Tetrahedron* **1964**, *20*, 2339.
- [45] M. L. Ślęczkowski, E. W. Meijer, A. R. A. Palmans, *Macromol. Rapid Commun.* **2017**, *38*, 1700566.
- [46] B. A. G. G. Lamers, M. L. Ślęczkowski, F. Wouters, T. A. P. P. Engels, E. W. Meijer, A. R. A. A. Palmans, *Polym. Chem.* **2020**, *11*, 2847.
- [47] D. J. Skrovanek, S. E. Howe, P. C. Painter, M. M. Coleman, *Macromolecules* **1985**, *18*, 1676.
- [48] X. C. Tang, M. J. Pikal, L. S. Taylor, *Pharm. Res.* **2002**, *19*, 484.
- [49] Y. Spiesschaert, C. Taplan, L. Stricker, M. Guerre, J. M. Winne, F. E. Du Prez, *Polym. Chem.* **2020**, *11*, 5377.
- [50] B. Diggle, Z. Jiang, R. W. Li, L. A. Connal, *Chem. Mater.* **2021**, *33*, 3712.
- [51] Y. Chen, H. Zhang, S. Majumdar, R. A. T. M. van Benthem, J. P. A. Heuts, R. P. Sijbesma, *Macromolecules* **2021**, *54*, 9703.
- [52] K. S. Fancey, *J. Mater. Sci.* **2005**, *40*, 4827.
- [53] G. Williams, D. C. Watts, *Trans. Faraday Soc.* **1970**, *66*, 80.
- [54] M. Delahaye, J. M. Winne, F. E. Du Prez, *J. Am. Chem. Soc.* **2019**, *141*, 15277.
- [55] S. Majumdar, B. Mezari, H. Zhang, J. van Aart, R. A. T. M. van Benthem, J. P. A. Heuts, R. P. Sijbesma, *Macromolecules* **2021**, *54*, 7955.
- [56] H. Zhang, S. Majumdar, R. A. T. M. van Benthem, R. P. Sijbesma, J. P. A. Heuts, *ACS Macro Lett.* **2020**, *9*, 272.
- [57] W. Denissen, G. Rivero, R. Nicolaÿ, L. Leibler, J. M. Winne, F. E. Du Prez, *Adv. Funct. Mater.* **2015**, *25*, 2451.

- [58] M. Röttger, T. Domenech, R. van der Weegen, A. Breuillac, R. Nicolaÿ, L. Leibler, *Science* **2017**, 356, 62.
- [59] D. Montarnal, M. Capelot, F. Tournilhac, L. Leibler, *Science* **2011**, 334, 965.
- [60] J. P. Brutman, P. A. Delgado, M. A. Hillmyer, *ACS Macro Lett.* **2014**, 3, 607.
- [61] Y. Zhou, J. G. P. Goossens, R. P. Sijbesma, J. P. A. Heuts, *Macromolecules* **2017**, 50, 6742.
- [62] M. M. Obadia, B. P. Mudraboyina, A. Serghei, D. Montarnal, E. Drockenmuller, *J. Am. Chem. Soc.* **2015**, 137, 6078.
- [63] O. Anaya, A. Jourdain, I. Antoniuk, H. Ben Romdhane, D. Montarnal, E. Drockenmuller, *Macromolecules* **2021**, 54, 3281.
- [64] E. E. L. Maassen, J. P. A. Heuts, R. P. Sijbesma, *Polym. Chem.* **2021**, 12, 3640.

SUPPORTING INFORMATION

Additional supporting information can be found online in the Supporting Information section at the end of this article.

How to cite this article: R. Sarkar, S. Majumdar, S. Kuil, J. Mallens, J. J. B. van der Tol, R. P. Sijbesma, J. P. A. Heuts, A. R. A. Palmans, *J. Polym. Sci.* **2023**, 61(13), 1335. <https://doi.org/10.1002/pol.20230068>